Journal of Engg. Research ICAPIE Special Issue pp. 257-272 DOI:10.36909/jer.ICAPIE.15069

WAMS Based Real-Time Voltage Stability Monitoring for Various Load Models in the Presence of a DFIG Integrated Wind Farm

Raju Chintakindi* and Arghya Mitra

Department of Electrical Engineering, Visvesvaraya National Institute of Technology, Nagpur, 440010, India.
**Corresponding Author: rajuphdvnit@gmail.com*

ABSTRACT

With rising global energy demand, transmission lines are operated at their limits, causing electrical grids to operate under extreme voltage instability conditions. To meet the increased load-demand and the forced tendency across the globe of tilting towards even more renewable generation, solar and wind farms are integrated with increased size and capacity. These uncontrolled natural power injection again may affect the system's voltage stability. To avoid blackouts and to achieve the maximum voltage stability of power systems, operators need to do effective real-time grid monitoring and control at load terminals. Load models are important in the analysis of voltage stability, and accurate load models are useful in analysing the voltage stability conditions. Phasor-measurement-unit (PMU) based wide-area monitoring and smart-automation is an innovative technology for measuring load voltage magnitude, phase angle, and frequency variations in a DFIG integrated large wind power system. This research paper focuses on estimating the real-time voltage stability through the use of linear, nonlinear, and dynamic load models in presence of a DFIG based wind-farm in WSCC three-machine nine-bus power network using PMU data. This study is carried out using MATLAB-Simulink software.

Keywords: WAMS; PMU; Voltage stability monitoring; Load modeling; DFIG integration.

INTRODUCTION

The voltage stability monitoring and analysis is the most significant function of a smart-grid operator to avoid the grid stress. The principal reasons for voltage instability are commonly, intermittent nature of power injection from a source of stochastic in nature, a sudden change or loss-of-load (LOL) in a particular location; or line tripping (LT) in a transmission system or some protective devices failure, etc. During a contingency, the network will experience voltage deviation, which may lead to total voltage collapse. The issue of voltage stabilization becomes critical with variation in different types of loads. Over the last few years, load modelling has become the most imperative aspect of power grid performance to withstand static and dynamic voltage fluctuations. Most commonly connected power system loads are linear, nonlinear, and dynamic in nature. It is essential to detect the vulnerable bus to take corrective action, empower the operator, and improve situational awareness (Biswas and Srivastava 2013).

Global positioning system (GPS) communication-based architecture is used for online tracking and regulation of a smart grid (Mahmoud and Barzegaran 2015). These measurements are more precise, synchronized with a positive sequence of voltage and current, phase angle, frequency, and rate-of-change of frequency (ROC-OF) with one microsecond accuracy (Goh et al. 2014). It can assess online voltage stability and provide alarms to grid operators, and thereby allowing them to take corrective action such as load shedding or automated restoration functions. The wide-area monitoring system is connected to power-generating units, substations and power grid control centers through a highly secure communication network. Using this new communication network, the grid operator can receive early indications of voltage error, or loss, and see the output waveform to look for whether the voltage limit is exceeded or not (Li, Bose, and Venkatasubramanian 2016).

The primary goal of this study is to create a novel measurement environment with time stamping measurements by using Synchrophasor aided technology; and assessing the effect of voltage fluctuations on static and dynamic load models for a power network incorporated with DFIG integrated wind-farm. Result shows the path through various load models to identify the weak buses and healthy buses. A new 'measurement-based approach' has used on the real-time PMU data samples to evaluate voltage stability condition. This article's novelty is that it introduces a technique for evaluating critical loads, weak buses, and load parameter values focused on their influence on the voltage-stability of the power systems. These simulation findings are very useful for the deployment of real-time wide-area monitoring and smart automation technology with renewable energy sources integration. We have divided this research into four major sections for simple demonstration. Section I discusses the functionality and communication network overview of the real time Wide Area Monitoring System (WAMS). Section II discusses the modelling and connection of a DFIG-integrated wind-farm (DFIG-WF) to the 230kV utility bus via a transformer. Section III discusses the load modeling and execution approach, as well as the flowchart of the measurement-based load modeling (MBLM) technique and the identified approach for dynamic-load model (DLM) processing. Section IV discusses WAMS based real-time voltage stability monitoring on linear, nonlinear and dynamic load models in the presence of DFIG integrated wind farm.

REAL-TIME WIDE AREA MONITORING SYSTEM USING PMU TECHNOLOGY

Power engineers are now prioritizing the use of measurement instruments with advanced detection and protection technology. Consequently, the practice of wide-area monitoring technology in today's electrical grid is becoming increasingly important. WAMS combines the roles of both traditional and new metering instruments with the functionality of communication networks to track, monitor, and regulate power networks across a large geographical area. A receiver circuit and an antenna generate 1PPS synchronized waveform in the GPS device.

Figure 1. shows the location of PMUs in specified load areas, such as industry, farming, and residential areas, in real time using the Synchrophasor based WAMS Technology.

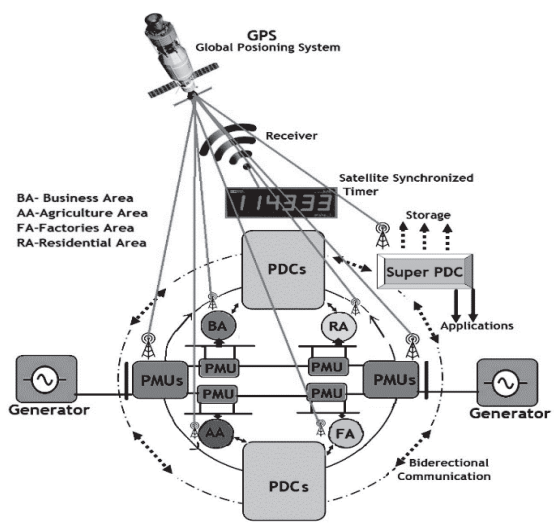

Figure 1. Synchrophasor technology-based online wide-area tracking system (Chintakindi and Mitra 2020).

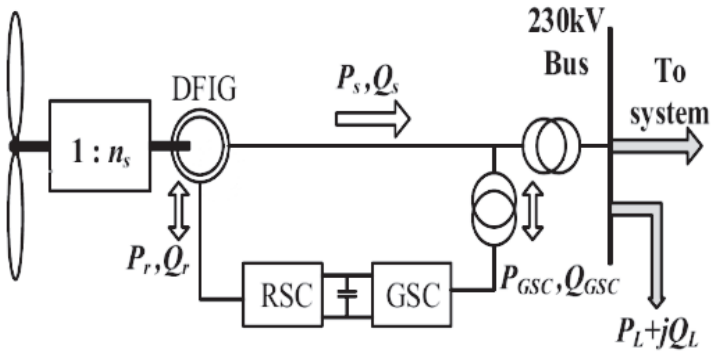

Figure 2. The multi-machine electricity network was being integrated with the 100 MW DFIG rated wind farm.

DOUBLY FED INDUCTION GENERATOR BASED WIND FARM

In recent years, the amount of wind-power-penetration (WPP) has increased significantly. DFIGs have been used as a wind generator in most of the wind farms. A number of methods in relation to the DFIG reactive-power functionality curve have been developed in (Engelhardt, S., Erlich, I., Feltes 2011), making it crucial as one of the major factor in relation to voltage stability lies with the amount of reactive-power exchange with the power grid. The DFIG reactive power capability using rotor-side-converters (RSC) and grid-side-converters (GSC) was examined in (Kayikci, M., Milanovic 2007). A dual-circuit line and a transformer are used to connect a DFIG to the system load bus (Kling, n.d. 2004). The DFIG-connected grid is depicted in detail in Figure 2. It shows how a transformer is used to link a DFIG-WF to a 230kV utility bus. The wind-turbine (WT) is coupled to the DFIG via a gearbox with a gearbox ratio ns. Here, Ps and Qs denote the active and reactive-power flows through the machine stator winding and Pr and Qr are transmitted through the rotor. The drive train model of the wind farm along with the mathematical representation of the DFIG can be found in (Mitra and Chatterjee 2016).

The total actual and reactive-power exchanged by DFIG with the power network can be calculated as follows:

$$P_{tot}=P_s+P_r=V_{ds}\, i_{ds}+V_{qs}\, i_{qs}+V_{dr}\, i_{dr}+V_{qr}\, i_{qr} \quad (1)$$

$$Q_{tot}=Q_s+Q_{GSC}=V_{qs}\, i_{ds}-V_{ds}\, i_{qs} \quad (2)$$

Where V_{qs}, V_{ds} & V_{qr},V_{dr} stand for q-axis, and d-axis voltage levels of the stator and rotor, respectively. i_{qs}, i_{ds} & i_{qr},i_{dr} stand for q-axis, and d-axis current levels of the stator and rotor circuit respectively. Q_{GSC} stands for reactive power through GSC. The DFIG's stator is coupled to the power-grid directly, whereas the rotor is coupled to the power-grid through an AC/DC/AC converter. The wind-speed is kept at 15 m/s, which is the rated speed. The rotor rated speed for 1 p.u. active power generation is 1.2 p.u. The reactive-power generated by the DFIG is considered as zero.

EXECUTION OF LOAD MODELING CONCEPT

PMU-assisted load modeling (LM) has recently been recognized as an significant aspect of power systems modeling (Price W, Chiang H-D, Clark-H, Concordia C, Lee-D, Hsu J, Ihara S, King-C, Lin-C and Y. 1993). Adequate specific load-models (LMs) are critical to avoid the grid collapsing and fragmenting during fluctuations. To accurately test the behaviour of the transmission system and provide directions for post-fault operations, a detailed implementation of LMs in the modern power-system is required (Milanovic JV, Gaikwad-A, Borghetti A, Djokic-SZ, Dong-ZY, Andrew-

Halley, Villanueva SN, Ma J, Pourbeik P, Resende F, Sterpu S, Villella F, Yamashita K, Auer O, and K, Kosterev D, Leung SK, Mtolo D, Zali SM, Collin A 2014). Load modelling has many advantages, such as, voltage-dependent energy consumption; active and reactive-power demand estimation for individual buses; controlling the magnitude of the load bus, reducing losses, and improving the voltage profile are all things that can be done. Load models show that the load characteristics are the algebraic functions of the magnitude of voltage, frequency of the bus, and the power consumed; as shown in (3).

$$P = P_0 \left[\frac{V}{V_0}\right]^{\alpha_v} \left[\frac{f}{f_0}\right]^{\alpha_f} \tag{3}$$

Here, V0, f0, P0, Q0, are the primary state voltage, frequency, active and reactive power.

A static model displays the features of the load at a certain moment as algebraic-functions of both the frequency and voltage magnitude of the bus. Its parameters are defined in (4) (Arif et al. 2017).

$$k_{pv} = \frac{\frac{\Delta P}{P_0}}{\frac{\Delta V}{V_0}} \quad k_{qv} = \frac{\frac{\Delta Q}{Q_0}}{\frac{\Delta V}{V_0}} \quad k_{pf} = \frac{\frac{\Delta P}{P_0}}{\frac{\Delta f}{f_0}} \quad k_{qf} = \frac{\frac{\Delta Q}{Q_0}}{\frac{\Delta f}{f_0}} \tag{4}$$

The voltage and frequency sensitivity variables of the model are kpv, kqv, kpf, kqf. The power varies explicitly with its voltage magnitude in constant current load models.

$$P = P_0 \left(\frac{V}{V_0}\right)^2 \quad Q = Q_0 \left(\frac{V}{V_0}\right)^2 \tag{5}$$

$$P = P_0 \left(\frac{V}{V_0}\right) \quad Q = Q_0 \left(\frac{V}{V_0}\right) \tag{6}$$

Changes in voltage magnitude have no effect on the output power of a constant-power load.

$$P = P_0 \qquad Q = Q_0 \tag{7}$$

The polynomial load pattern defines the polynomial association of the power and voltage spectrum as a static load configuration. The ZIP model, comprises constant-impedance component (Z), constant-current component (I), and constant-power component (P). The voltage-based form of the polynomial-load model can be found in (Yue Zhu 2020)-(C W Taylor; Electric Power Research Institute - EPRI. (1993). As shown in (8) and (9), the power of a constant-impedance load is proportional to square of a bus voltage level, whereas the power of a constant-current load is directly proportional to the amount of bus voltage.

$$P = P_0 \left[p_1 \left(\frac{V}{V_0}\right)^2 + p_2 \left(\frac{V}{V_0}\right) + p_3\right] \tag{8}$$

$$Q = Q_0 \left[q_1 \left(\frac{V}{V_0}\right)^2 + q_2 \left(\frac{V}{V_0}\right) + q_3\right] \tag{9}$$

Where, V0 and P0 are the initial or nominal values of voltage and power for the system. The polynomial coefficients of load must satisfy the conditions as shown in (10) and (11).

$$p_1 + p_2 + p_3 = 1 \tag{10}$$

$$q_1 + q_2 + q_3 = 1 \tag{11}$$

The variables q1, and p1 represent the percentage of Z; q2, and p2 denote the percentage of I; and q3 and p3 denote the P percentage of the total load combination. The sum of these parameters (p1, p2, p3, and q1, q2, q3) must be individually equal to 1. Figure 3 shows the role of reducing the two-bus network for ZIP loads for the network with a 2 bus constant-power load elements. Here, $\bar{E}$=E$\angle 0^0$ and $\bar{V}$=V$\angle\theta$. The ($\bar{I}_L$) and ($\bar{Z}_L$) load elements are specified, in a ZIP load concept (Borka Milˇosevic 2003). The static-exponential-load (SEL) pattern is among the most widely used load configurations in recent times (Yue Zhu 2020). This loading pattern is an exponential function, as shown in (12), which defines the power relation to voltage.

$$P = P_0 \left(\frac{V}{V_0}\right)^{np} \quad Q = Q_0 \left(\frac{V}{V_0}\right)^{nq} \tag{12}$$

Here, P is the load point active power, and Q is the reactive power, np and nq are model's variables. The dynamic load model illustrates how the load operates, in which real and reactive-power rely on frequency, voltage, which are vary with time. The dynamic-load configurations include the composite loading pattern, exponential-dynamic, and dynamic induction-motor. An exponential dynamic-load approach is suggested in (S. S. Biswas, C. B. Vellaithurai 2013), which shows it as a collection of non-linear equations, as in (13).

$$T_p \frac{dP_r}{dt} + P_r = P_s(V) + P_t(V) = P_0 \left(\frac{V}{V_0}\right)^{\alpha_s} - P_0 \left(\frac{V}{V_0}\right)^{\alpha_t} \tag{13}$$

Where, Tp is the time constant for real-power recovery, Pr is the restoration of actual power, P0 is the primary actual-power flow before the voltage-change, V0 is the primary voltage level, αs is the steady state active-power voltage exponent. αt is the transitory active-power voltage exponent, and PL is utilization of active-power.

$$T_q \frac{dQ_r}{dt} + Q_r = Q_s(V) + Q_t(V) = Q_0 \left(\frac{V}{V_0}\right)^{\beta_s} - Q_0 \left(\frac{V}{V_0}\right)^{\beta_t} \tag{14}$$

$$Q_l = Q_r + Q_0 \left(\frac{V}{V_0}\right)^{\beta_t} \tag{15}$$

T_q the time constant for reactive-power recovery; Q_r is restoration of reactive-power; Q_0 is primary power reactive-flow before voltage change; β_s is a steady state reactive-power voltage exponent; β_t is transitory reactive-power voltage exponent; and Q_L is utilization of reactive-power. Figure 4 shows the exponential dynamic-load configuration performance. It shows the structure of the reaction after a voltage condition and the physical significance of the variables. In (Tomiyama-K, Ueoka S, Takano-T, Iyoda I, Matsuno-K, Temma K. 2003), it is shown that after a small voltage variation in the induction motor operation, the model accurately describes the long-term load impacts. Figure 5 shows the measurement-based load modeling technique in a flowchart form. It is useful for determining the load module's voltage deviation, active, and reactive-power streams in the grid. This method can be used to test and evaluate the real loads. The power grid is looking into new options or better load models to counteract the vulnerabilities. Figure 6 shows the processing schematic diagram for the dynamical load model in a flowchart form. The load shift will lead to a change in the power source frequency, with the induction motor and frequency-dependent power electronic circuits.

Dynamic-load configuration has been used for risk reduction, reliability, and quality enhancement (Rahman 2013).

VOLTAGE STABILITY MONITORING IN THE PRESECE OF A DFIG INTEGRATED WIND FARM

Voltage instability will occur if any one of the load unexpectedly rises in the highly loaded network, which results in the abrupt decrease of grid voltage. To avoid this, smart grid engineers and service providers must always operate the grid in a sufficient distance away from the voltage-stability boundary. PMUs are used t measure real-time voltage deviations on various load and generator terminals (Goh et al. 2014). Figure 7 displays a three-machine nine-bus power-grid diagram (Chatterjee, n.d. 2012). Wind farm is normally located in an area with plenty of wind speed. In the 9-bus system, it could be integrated into one of the three load buses. In the figure, bus 7 has considered as the point of connection of windfarm. Here, a 100 MW wind power plant is considered, involving of sixty-seven 1.5 MW wind-turbines (WTs). To meet the additional load demand, we integrated the DFIG based wind farm with the existing system. The wind farm's output was adjusted to match the additional load connected to the network. Because both the additional load and the wind farm are connected to the same bus, there was no change in the power network's steady-state load-flow after the wind farm was integrated (Mitra and Chatterjee 2016). Figure 8 and 9 show the output voltage and power waveforms of the 100 MW DFIG when connected to bus 8. PMUs monitor online voltage phasors. The per unit value of the voltage at bus 8 is almost unity (as it was after the integration of wind-farm), and the real power generation by the wind-farm was recorded at 100 MW, as can be seen from the Figures 8 and 9.

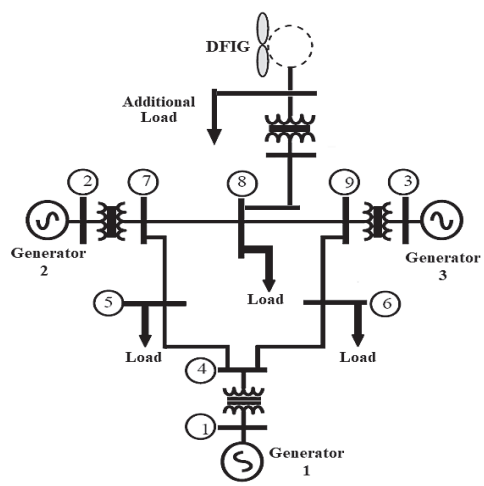

Figure 7. Proposed online diagram for a nine-bus power grid with DFIG-based wind farm integration at bus 8.

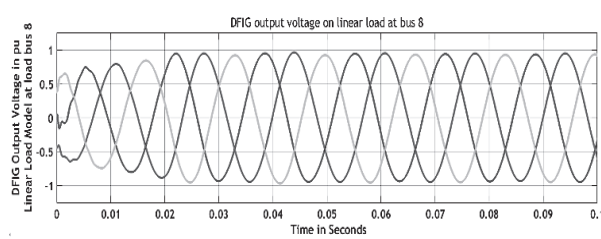

Figure 8. Waveforms of 100 MW DFIG output voltage which were integrated at bus 8

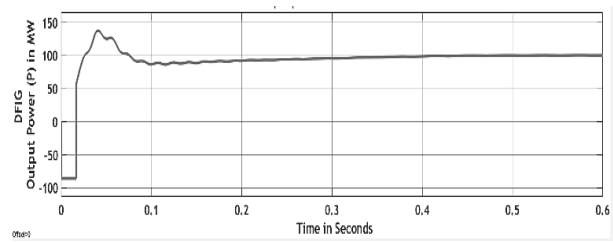

Figure 9. Waveforms of 100 MW DFIG output power which were integrated at bus 8.

Real-time Voltage Stability Monitoring on Linear Load Model with DFIG Integration

Normally in power transmission system, steady state voltage limit is considered between 0.95 – 1.05 pu. There is no recommendations required, if the magnitude of the voltage is between 0.95 and 1.05 pu. There will be an indication through an alarm whenever the voltage of the monitored bus exceeds the specified limit. Tables 1, 2, and 3 show the measured voltage, current magnitudes, and phase angles for a linear load model at bus 5, 6, and 8.

Table 1. Identified voltage, current magnitudes, and phase angles for a Linear load model at bus 5

PMU Recordings with Time Stamping Technology					
Samples	**Time Stampings (t and t' in sec.)**	**Voltage-Magnitude (pu)**	**Voltage-Angle (degrees)**	**Current-Magnitude (pu)**	**Current-Angle (degrees)**
1	0.19491500000000 2.417688529635757	0.965436885473423	6.567481248864803	0.883216400452475	
2	0.19505300000000 2.430331567460585	0.965446501474170	6.584485814528143	0.883270039296813	
3	0.19531300000000 2.442847860415699	0.965457306276394	6.601619421787158	0.883321586874768	
4	0.19557300000000 2.458567334824225	0.965468399928401	6.622437410504410	0.883368641976598	
5	0.19583400000000 2.474139060806917	0.965479286651066	6.643645130336871	0.883410215968259	

Table 2. Identified voltage, current magnitudes, and phase angles for a Linear load model at bus 6

PMU Recordings with Time Stamping Technology					
Samples	**Time Stampings (t and t' in sec.)**	**Voltage-Magnitude (pu)**	**Voltage-Angle (degrees)**	**Current-Magnitude (pu)**	**Current-Angle (degrees)**
1	0.19491500000000	0.982857420100081	6.671743725218922	0.613175570135173	3.33025573065621
2	0.19505300000000	0.982865524706251	6.688942364349312	0.613233461488255	3.314858103688139
3	0.19531300000000	0.982874789899573	6.706263655941310	0.613290505292569	3.299604114014448
4	0.19557300000000	0.982884315022277	6.727264455861686	0.613344630735689	3.281197280608202
5	0.19583400000000	0.982893596044645	6.748650690788633	0.613395089629003	3.263002961358339

Table 3. Identified voltage, current magnitudes, and phase angles for a Linear load model at bus 8

PMU Recordings with Time Stamping Technology					
Samples	**Time Stampings (t and t' in Sec.)**	**Voltage-Magnitude (pu)**	**Voltage-Angle (degrees)**	**Current-Magnitude (pu)**	**Current-Angle (degrees)**
1	0.19505200000000	0.978621926343958	11.752828063325016	`0.770285575238991	3.469613468531489
2	0.19505300000000	0.978654485536288	11.769588960582658	0.770339627707702	3.507698026407756
3	0.19531300000000	0.978688590184016	11.786435264355955	0.770403794600000	3.545169674607851
4	0.19557300000000	0.978722726157995	11.806917053811652	0.770478490231112	3.585977231546291
5	0.19583400000000	0.978756417038358	11.827730818767860	0.770561878213858	3.627142795557613

By using time stamping technology on linear load model, PMU identified that, 125 MW, 50 MVar rated load bus 5 has less voltage magnitude than that of the load buses 6 and 8. Correspondingly, Figure 10 depicts the magnitude of the identified low voltage at bus 5.

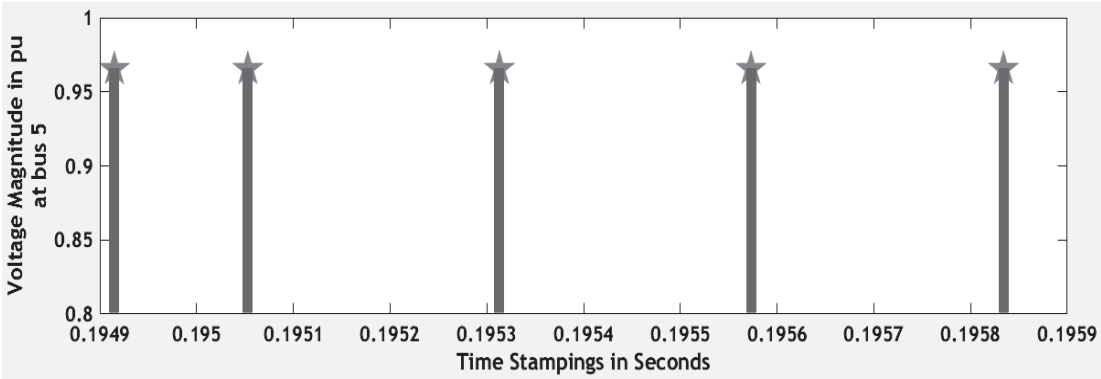

Figure 10. The voltage magnitude of a PMU data on the linear load at bus 5.

Real-time Voltage Stability Monitoring on Non-Linear Load Model with DFIG Integration

The Universal-Bridge is the basic building block of a dual-level voltage-source-converters (VSC) (Sadamoto et al., 2018), which is used as a nonlinear load model. The Universal Bridge block simulates converters can use both line-commutated (and naturally commutated) and forced-commutated semi-conductor devices (GTO, IGBT, MOSFET). Tables 4, 5, and 6 show the measured voltage, current magnitudes, and phase angles for a nonlinear load model on bus 5, 6, and 8.

Table 4. Identified voltage, current magnitudes, and phase angles for a Nonlinear load model at bus 5

PMU Recordings with Time Stamping Technology					
Samples	**Time Stampings (t and t' in sec.)**	**Voltage-Magnitude (pu)**	**Voltage-Angle (degrees)**	**Current-Magnitude (pu)**	**Current-Angle (degrees)**
1	0.194916000000 54.948298830710307	0.938904327072365	-80.703649789254328	1.626579526694328	-
2	0.195053000000 55.121547436616261	0.939041400981494	-80.847249110888171	1.626604552476471	-
3	0.195313000000 55.290773090777073	0.939058074875963	-80.992366334765890	1.626887076862606	-
4	0.195573000000 55.457633922923961	0.939129741536335	-81.134777052079315	1.627339800522255	-
5	0.195834000000 55.621893213511200	0.939177264062648	-81.273371282752237	1.628128918093122	-

Table 5. Identified voltage, current magnitudes, and phase angles for a Nonlinear load model at bus 6

PMU Recordings with Time Stamping Technology					
Samples	**Time Stampings (t and t' in sec.)**	**Voltage-Magnitude (pu)**	**Voltage-Angle (degrees)**	**Current-Magnitude (pu)**	**Current-Angle (degrees)**
1	0.194915000000 59.728362641494002	0.960479355030300	-79.211121897164944	1.23783588838639	-
2	0.195053000000 59.899323862052896	0.960588731348874	-79.353068955405490	1.237784617055960	-
3	0.195313000000 60.061959303915472	0.960552442060620	-79.498668131514449	1.237980432075984	-
4	0.195573000000 60.223825130995145	0.960567762158723	-79.640964998421055	1.238340241749240	-
5	0.195834000000 60.386018715279995	0.960612514269223	-79.779418487611622	1.238991555197455	-

Table 6. Identified voltage, current magnitudes, and phase angles for a Nonlinear load model at bus 8

PMU Recordings with Time Stamping Technology					
Samples	**Time Stampings Angle (t and t' in Sec.)**	**Voltage-Magnitude (pu)**	**Voltage-Angle (degrees)**	**Current-Magnitude (pu)**	**Current- (degrees)**
1	0.194915000000 53.478021200939551	0.903739145798336	-68.094008961506603	0.965977248307560	-
2	0.195053000000 53.610997381915531	0.903818243708580	-68.233324791986632	0.965294311710787	-
3	0.195313000000 53.752169336246475	0.903796933751164	-68.379047749890418	0.964903629050897	-
4	0.195573000000 53.886658304934940	0.903741823639970	-68.522320119036991	0.964873984591000	-
5	0.195834000000 54.008866428353535	0.903618544218108	-68.662650307731511	0.964877989962595	-

By using time stamping technology on nonlinear load model, PMU identified that, 90 MW, 30 MVar rated load bus 8 has less voltage magnitude than that of the load buses 5 and 6. Correspondingly, Figure 11 depicts the magnitude of the identified low voltage at bus 8. The key cause of voltage degradation is the poor reactive-power supply. It is because of rapid change in the network components to divert power streams and/or the increasing rise in energy demand in a way where certain buses' VAR needs cannot fulfilled locally. Although the steady-state voltage volatility, primarily for progressive VAR deficiency, can control by the network operators' and utilities' timely operation.

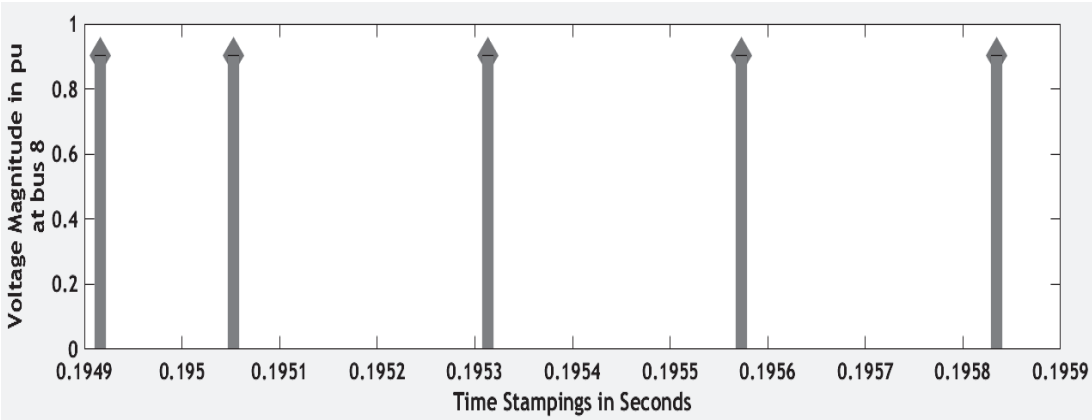

Real-time Voltage Stability Monitoring on Dynamic Load Model with DFIG Integration

The three-phase dynamic-load-block executes 3-Φ, 3-wire dynamical load, whose P and Q change in relation with positive-sequence voltage. Zero and negative-sequence currents need not to be simulated. As a result, the three load currents are equally distributed. The load-impedance is kept constant if the terminal voltage (Vt) of the load is less than the minimum rated value (Vmin). This section explores the effect on the voltage stability cases of a 3-phase induction motor based on load modeling. All these dynamic-load models being integrated on base-power (VA 3 phase) are 100 MVA and the rated voltage level is 230 kV. Tables 7, 8, and 9 show the measured voltage, current magnitudes, and phase angles for a dynamic load model at bus 5, 6, and 8.

Table 7. Identified voltage, current magnitudes, and phase angles for a Dynamic load model at bus 5

PMU Recordings with Time Stamping Technology					
Samples	**Time Stampings (t and t' in sec.)**	**Voltage-Magnitude (pu)**	**Voltage-Angle (degrees)**	**Current-Magnitude (pu)**	**Current-Angle (degrees)**
1	0.194915000000000	0.947178473939668	0.260555751765131	0.914303822082440	-3.757328744973985
2	0.195053000000000	0.946039485432303	0.195862373442168	0.904195295670318	-4.079731276246574
3	0.195313000000000	0.952444897958461	0.397290233515864	0.901341707774578	-4.223397861927534
4	0.195573000000000	0.953190331828783	0.528354315577356	0.910544871675745	-3.795941203903757
5	0.195834000000000	0.947500472225353	0.360407686124303	0.911379953866048	-3.416145412211377

Table 8. Identified voltage, current magnitudes, and phase angles for a Dynamic load model at bus 6

PMU Recordings with Time Stamping Technology					
Samples	**Time Stampings (t and t' in seconds)**	**Voltage-Magnitude (pu)**	**Voltage-Angle (degrees)**	**Current-Magnitude (pu)**	**Current-Angle (degrees)**
1	0.19491500000000	0.965794731072534	0.601600745117837	0.640184691616401	-10.212832872372593
2	0.19505300000000	0.964918635510519	0.555426418478807	0.628304289444156	-10.698823174422381
3	0.19531300000000	0.969896714837361	0.711853973849234	0.623364114666033	-10.893997099220316
4	0.19557300000000	0.970462996358495	0.816241215866405	0.633009741017082	-10.263912611068543
5	0.19583400000000	0.966057131850665	0.693041633555090	0.635611212158283	-9.739180319294174

Table 9. Identified voltage, current magnitudes, and phase angles for a Dynamic load model at bus 8

PMU Recordings with Time Stamping Technology					
Samples	**Time Stampings (t and t' in Seconds)**	**Voltage-Magnitude (pu)**	**Voltage-Angle (degrees)**	**Current-Magnitude (pu)**	**Current-Angle (degrees)**
1	0.19491500000000	0.965975689368232	6.570527030635786	0.792998561888780	2.065554250843987
2	0.19505300000000	0.966577170386668	6.600879508507629	0.794341969001007	2.155041320901966
3	0.19531300000000	0.966920580857682	6.633692771659701	0.794782531405417	2.229526119587149
4	0.19557300000000	0.966320174095575	6.631082314793845	0.793600124720849	2.215599258984926
5	0.19583400000000	0.966150038524164	6.616262822883055	0.793520853522914	2.198219982110322

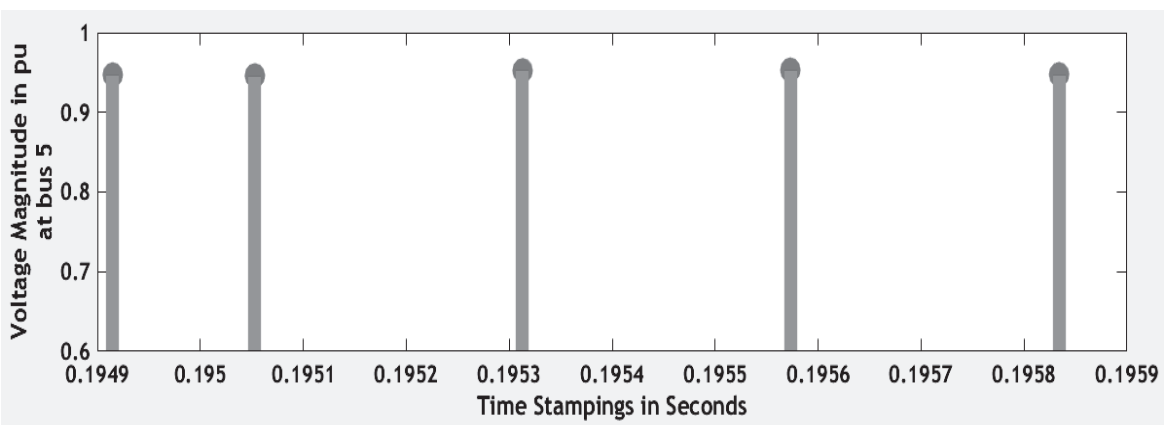

Figure. 12. The voltage magnitude of a PMU data on the dynamic load at bus 5.

Figure 12 represents the magnitude of identified low voltage on the bus 5. By using time stamping technology on dynamic load model, Synchophasor identified that, 125 MW, 50 MVar rated load bus 5 has less voltage magnitude than other load buses 6 and 8. Similarly, Figure 14 depicts the magnitude of the identified low voltage at bus 8.

Bus Ranking for Weak Bus Identification

Operators always maintain the voltage within defined levels (Kundur-P, Paserba-J, Ajjarapu-V, Andersson G, Bose-A, Canizares C, Hatziargyriou-N and Stankovic-A, Taylor-C, Van Cutsem-T 2004). The power system's inability to meet reactive-power demand in the overloaded network while keeping the voltage within the allowable range causes voltage instability. Figure 13 illustrates the magnitude of voltage variation on a linear load model for load buses 5, 6, and 8. On a linear load model, Synchrophasor time stampings technology was used to test 5 series of samples of different voltage magnitudes. According to PMU data, bus 6 has a voltage magnitude of nearly 0.985 pu, bus 8 has a voltage magnitude of less than 0.98 pu, and bus 5 has magnitude of voltage less than 0.965 pu. The bus 5 is most critical, and bus 6 is the most stable according to the PMU's recordings. As a result, additional incremental load on bus 5 is not recommended, while bus 6 is recommended for additional load or a distributed power generation alternative.

Figure 14 illustrates the magnitude of voltage variation on a nonlinear load model for load buses 5, 6, and 8. On a nonlinear load model, we also tested 5 series of samples of different voltage magnitudes. According to Synchrophasor data, bus 6 has a voltage magnitude of approximately 0.96 pu, bus 5 has a voltage magnitude of less than 0.94 pu, and bus 8 has a voltage magnitude nearly 0.9 pu. So, bus 8 is most critical, and bus 6 is the most stable, according to the Synchrophasor recordings. As a result, additional incremental load on bus 8 is not recommended, while bus 6 is recommended for additional load or a distributed power generation alternative.

Figure 15 illustrates the magnitude of voltage variation on a dynamic load model for load buses 5, 6, and 8. On a dynamic load model, Synchrophasor time stampings technology was used similarly to test 5 series of samples. According to PMU data, bus 6 has a voltage magnitude of nearly 0.97 pu, bus 8 has a voltage magnitude of less than 0.97 pu, and bus 5 is having a voltage magnitude which is found to be less than 0.95 pu. Therefore, bus 5 can be considered as most critical, and bus 6 is the most stable and healthy, according to the PMU's recordings. As a result, additional incremental load on bus 5 is not recommended, while bus 6 is recommended for additional load or a distributed power generation alternative.

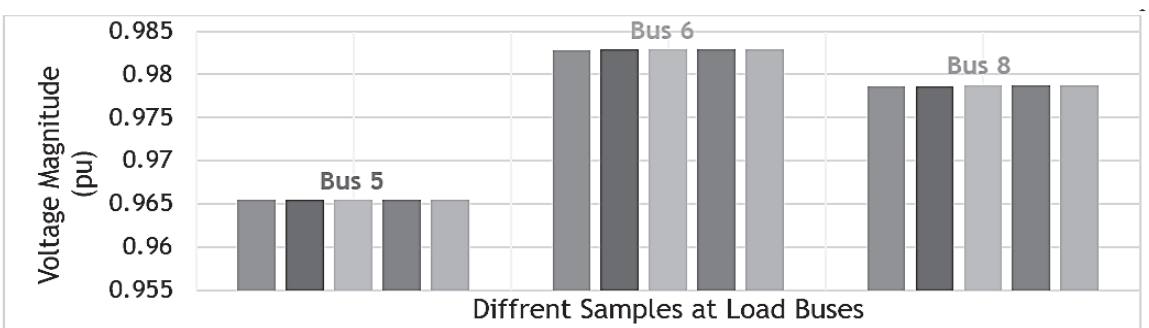

Figure. 13. Voltage magnitude variation on linear load-model on load buses 5, 6, 8.

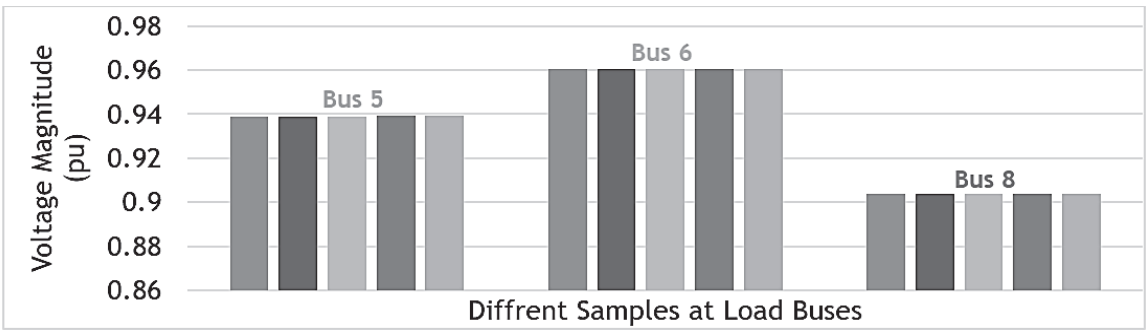

Figure. 14. Voltage magnitude variation on non-linear load-model on load buses 5, 6, 8.

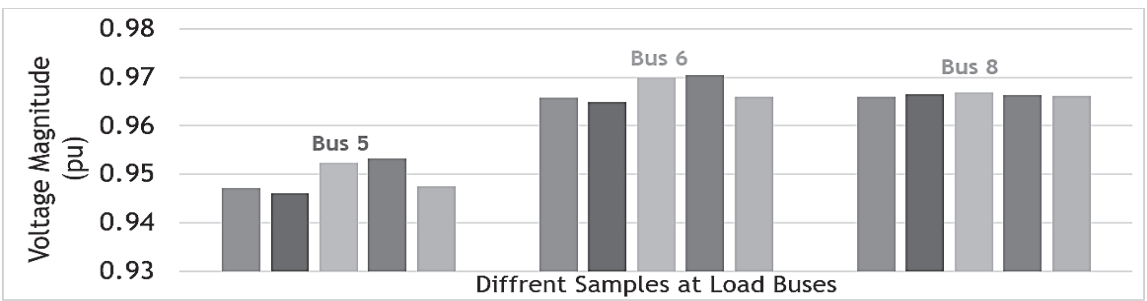

Figure. 15. Voltage magnitude variation on dynamic load-model on load buses 5, 6, 8.

In addition, when testing linear and dynamic load models, load bus 5 is more vulnerable than load bus 8. But the DFIG-based wind farm is integrated at bus 8, though it is observed that bus 8 is more critical than load buses 5 and 6 in nonlinear load model testing. It requires more situational awareness on bus 5 for the operator under real-time wide-area monitoring. The load positions away from the generators seem more significant. The transmission lines are responsible for some losses and the power can be consumed through the other interlinked load terminals. This loss of power on such generator buses would contribute to voltage declines on those buses, reducing the voltage stability of the system. This study gives the first way to detect vulnerable buses in a power system network. With each load variation used in the study, an alternative method is presented and examined for measuring the voltage stability using PMUs. This similarity analysis has identified the strained state of the transmission lines and established the vulnerable areas susceptible to failure according to the voltage-stability.

CONCLUSION

In the presence of a DFIG-based wind farm, steady-state voltage stability analysis on linear, non-linear, and dynamic load models using a PMU-based real-time WAMS technology is performed. In real-time loading scenarios, the voltage magnitude, phase angle, and frequency profiles were recorded. A novel measurement-based approach has demonstrated with the help of flowcharts for load modeling and voltage stability analysis. In the electrical power grid monitoring, this comparative analysis can forecast voltage failure, from the steady state condition of the transmission lines. It is determining the vulnerable bus areas susceptible to voltage collapse based on the ranking of load buses on various load models. These results are highly accurate because of the use of PMU data analytics. This investigation is useful for determining the most effective countermeasures to voltage instability, and proper planning can be organised based on system capacity to prevent voltage collapse.

This study also enables the network operators to schedule production re-dispatch instructions in order to avoid load curtailments. Recommendations for FACTS, or other reactive power compensating devices can mount in the weakest regions of the system. In the long-run, the findings of this study could be useful for a variety of other stability-related issues, such as verifying real-time voltage stability, reactive power injection, and voltage restoration.

REFERENCES

Arif, Anmar, Zhaoyu-Wang, Jianhui-Wang, Barry-Mather, Hugo-Bashualdo, and Dongbo-Zhao. 2017. "Load Modeling – A Review." IEEE Transactions on Smart Grid 9 (6): 5986–99.

Biswas, Saugata S., and Anurag K. Srivastava. 2013. "A Novel Method for Distributed Real Time Voltage Stability Monitoring Using Synchrophasor Measurements." Symposium-Bulk Power System Dynamics and Control. Rethymnon, Greece: IEEE Xplore Press. https://doi.org/10.1109/IREP.2013.6629377.

Borka Milˇosevic, Mirˇoslav Begovic. 2003. "Voltage-Stability Protection and Control Using a Wide-Area Network of Phasor Measurements." IEEE Transactions on Power Systems 18 (1).

C W Taylor; Electric Power Research Institute. - EPRI. 1993. Power System Voltage Stability. New York, NY: McGraw-Hill, 1994.

Chatterjee Dheeman and Arghya Mitra. 2012. "A New Sensitivity Based Approach to Study Impact of Wind Power Penetration on Transient Stability." IEEE International Conference on Power Electronics, Drives and Energy Systems (PEDES). Bengaluru, India: IEEE.

Chintakindi Raju, and Arghya Mitra. 2020. "Execution of Real-Time Wide Area Monitoring System with Big Data Functions and Practices." PIICON 2020 - 9th IEEE Power India International Conference. SONEPAT, India, India: IEEE.

Engelhardt, S., Erlich, I., Feltes, C. 2011. "Reactive Power Capability of Wind Turbines Based on Doubly Fed Induction Generators." IEEE Trans. Energy Convers 26: 364–72.

Goh, H. H., Q. S. Chua, S. W. Lee, B. C. Kok, K. C. Goh, and K. T.K. Teo. 2014. "Power Stability Monitoring Based on Voltage Instability Prediction Approach through Wide Area System." American Journal of Applied Sciences 11 (5): 717–31.

Kayikci, M., Milanovic, J.V. 2007. "Reactive Power Control Strategies for DFIG Based Plants." IEEE Trans. Energy Convers 22: 389–96.

Kling, J.G. Slootweg and W.L. 2004. "Impacts of Distributed Generation on Power System Transient Stability." EEE PES General Meeting, 2150–55.

Kundur P, Paserba J, Ajjarapu V, Andersson G, Bose A, Canizares C, Hatziargyriou N, Hill D, and Vittal V Stankovic A, Taylor C, Van Cutsem T. 2004. "Definition and Classification of Power System Stability IEEE/CIGRE Joint Task Force on Stability Terms and Definitions." IEEE Transactions on Power Power Systems, 19:1387–1401.

Li, Haoen, Anjan Bose, and Vaithianathan Mani Venkatasubramanian. 2016. "Wide-Area Voltage Monitoring and Optimization." IEEE Transactions on Smart Grid 7 (2): 785–93. https://doi.org/10.1109/TSG.2015.2467215.

Mahmoud, Hazzaz, and Mohammad Reza Barzegaran. 2015. "Hardware-in-the-Loop Wide Area Monitoring Protection and Control Using Software Based PMU's Model." Computational Research Progress in Applied Science & Engineering 01 (September): 141–51.

Milanovic JV, Gaikwad A, Borghetti A, Djokic SZ, Dong ZY, Andrew Halley, Korunovic LM, Karoui Villanueva SN, Ma J, Pourbeik P, Resende F, Sterpu S, Villella F, Yamashita K, Auer O, and XuY K, Kosterev D, Leung SK, Mtolo D, Zali SM, Collin A. 2014. "Modelling and Aggregation of Loads in Flexible Power Networks." J. M. CIGRE WG C4.605.

Mitra, Arghya, and Chatterjee, Dheeman. 2016. "Active Power Control of Dfig-Based Wind Farm for Improvement of Transient Stability of Power Systems." IEEE Transactions on Power Systems 31 (1): 82–93.

Price W, Chiang H-D, Clark H, Concordia C, Lee D, Hsu J, Ihara S, King C, Lin C, Mansour, and Y. 1993. "Load Representation for Dynamic Performance Analysis." IEEE Transactions on Power Systems, 8:472–482.

Rahman, Azizan Bin Haji Abd. 2013. "Simulation of Dynamic Load Effect on Power System Frequency."

S. S. Biswas, C. B. Vellaithurai, A. K. Srivastava. 2013. "Development and Real Time Implementation of a Synchrophasor Based Fast Voltage Stability Monitoring Algorithm with Consideration of Load Models." In IEEE Industry Applications Society Annual Meeting, 1–9.

Sadamoto, Tomonori, Aranya Chakrabortty, Takayuki Ishizaki, and Jun-ichi Imura. 2018. "Dynamic Modeling, Stability, and Control of Power Systems with Distributed Energy Resources." IEEE Control Systems Magazine 39 (2): 34–65. https://doi.org/10.1109/MCS.2018.2888680.

Tomiyama K, Ueoka S, Takano T, Iyoda I, Matsuno K, Temma K, Paserba JJ. 2003. "Modeling of Load during and after System Faults Based on Actual Field Data." Power Engineering Society General Meeting, IEEE, Pp 1385–1391.

Yue Zhu. 2020. Power System Loads and Power System Stability. 1st ed. Springer Nature Switzerland AG: Springer International Publishing. https://doi.org/10.1007/978-3-030-37786-1.